Available online at www.sciencedirect.com
SCIENCE DIRECT®
Journal of Computational Physics 210 (2005) 730–751
JOURNAL OF COMPUTATIONAL PHYSICS
www.elsevier.com/locate/jcp

A numerical scheme for the integration of the Vlasov–Poisson system of equations, in the magnetized case

Francesco Valentini [a,*], Pierluigi Veltri [a], André Mangeney [b]

[a] *Dipartimento di Fisica and Istituto Nazionale di Fisica della Materia, Universitá della Calabria, Ponte P. Bucci Cubo 31C, 87036 Rende (CS), Italy*
[b] *LESIA – Observatoire de Paris, Section de Meudon 5, place Jules Janssen, 92195 Meudon Cedex, France*

Received 5 November 2004; received in revised form 24 March 2005; accepted 11 May 2005
Available online 12 July 2005

Abstract

We present a numerical algorithm for the solution of the Vlasov–Poisson system of equations, in the magnetized case. The numerical integration is performed using the well-known "splitting" method in the electrostatic approximation, coupled with a finite difference upwind scheme; finally the algorithm provides second order accuracy in space and time. The cylindrical geometry is used in the velocity space, in order to describe the rotation of the particles around the direction of the external uniform magnetic field.

Using polar coordinates, the integration of the Vlasov equation is very simplified in the velocity space with respect to the cartesian geometry, because the rotation in the velocity cartesian space corresponds to a translation along the azimuthal angle in the cylindrical reference frame. The scheme is intrinsically symplectic and significatively simpler to implement, with respect to a cartesian one. The numerical integration is shown in detail and several conservation tests are presented, in order to control the numerical accuracy of the code and the time evolution of the entropy, strictly related to the filamentation problem for a kinetic model, is discussed.

PACS: 65N06; 82D10

Keywords: Vlasov; Splitting; Upwind; Damping; Bernstein; Filamentation

1. Introduction

In collisionless approximation, the Vlasov equation describes the time evolution of the distribution function, in the six-dimensional phase space, under the effect of the self-consistent and external electromagnetic

* Corresponding author. Tel.: +39 0984 496129; fax: +39 0984 494401.
E-mail address: valentin@fis.unical.it (F. Valentini).

0021-9991/$ - see front matter © 2005 Elsevier Inc. All rights reserved.
doi:10.1016/j.jcp.2005.05.014

fields, solutions of the Maxwell equations. In this way, the Vlasov–Maxwell system provides a powerful description of the plasma state, which depends on the details of the velocity distribution function. The interest of such an approach resides principally in the possibility to study the fundamental hamiltonian aspects underlying the nonlinear dynamics of collisionless plasma systems, taking into account particle effects (as wave–particle interactions), which are ruled out from fluid description, but play a fundamental role in particle acceleration and wave absorption phenomena, especially in collisionless plasmas. The Vlasov equation is a nonlinear partial derivative differential equation, whose analytical solution is available only in a few simplified linear cases, but the nonlinear regime, including the most interesting physical phenomena, must be investigated numerically.

In this context, particle in cell codes (PIC) [1] represent historically widely adopted approach to numerical simulations of plasmas in the framework of the kinetic theory and in the past years they have been considered the most effective tool in the description of the plasma dynamics, above all because such an approach allows to study a large panorama of physical aspects in the full dimensional case, with a relatively small computational costs. On the other hand, even if nowadays the computational effort is directed to use the modern massive parallel computers, in order to study numerically the solutions of the Vlasov–Maxwell system in the fully nonlinear regime, the six-dimensional phase space description is still a very hard goal. In spite of these considerations, a huge scenario of physical processes in plasma physics can be described in a phase space of lower dimensions and here Vlasov codes are extremely useful, for example in one spatial and one velocity coordinates phase space, one spatial and two velocity or in the four-dimensional description, with a relatively good numerical resolution. Moreover, using Vlasov codes allows to cancel the statistical noise which is intrinsic to PIC simulations.

The code presented in this paper solves numerically the Vlasov–Poisson system of equations in a three-dimensional phase space, one-dimensional in the physical space ($1D$) and two-dimensional in the velocity ($2V$). The numerical integration is based on the coupling of the splitting method, in electrostatic approximation [2], with a finite difference upwind scheme. The approach is similar to the "flux balance method" proposed by Fijalkow [3–5]. The algorithm is second order accurate in space and time. The peculiarity of the algorithm we have built up consists in using the cylindrical geometry in the velocity space, as we will discuss in detail in the next section. This geometry is particularly effective in describing the dynamics of charged particles moving in a plane perpendicular to a uniform magnetic field, because it represents the natural way to describe circular motions. Due to the fact that the rotation in the velocity cartesian space corresponds to a translation along the azimuthal angle in a polar reference frame, the numerical integration of the Vlasov equation, based on following the information flux, as required by the finite difference upwind scheme, results very simplified in cylindrical geometry with respect to the cartesian case. Moreover, using polar coordinates allows to obtain a numerical scheme intrinsically symplectic and simpler than a cartesian one, from the point of view of the code implementation.

As we will discuss in the next sections, the typical invariants of the Vlasov equation are conserved in time in a very satisfactory way, in the sense that the numerical fluctuations of these quantities, due to the discretization of the domain, are about two orders of magnitude smaller than the physical fluctuations, in a typical run, indicating that the numerical dissipation does not affect significatively the numerical results. In the present configuration, the code is suitable to describe the time evolution of electrostatic modes, propagating strictly perpendicular to an external uniform magnetic field, as the well-known Bernstein waves.

The paper is organized as follows. In Section 2, the Vlasov equation in cylindrical geometry is discussed and a short recall to the splitting method and to the integration of the *hyperbolic equations* is presented; a significative comparison between the cylindrical scheme and the cartesian ones is discussed. Section 3 is devoted to the numerical integration of the Vlasov equation in $1D - 2V$ phase space. In Section 4, we analyze the scaling of the truncation error with the simulation parameters and several conservation tests are discussed and compared with the theoretical predictions, to demonstrate that the numerical results are reliable. In Section 5, the numerical study of the entropy conservation in the Vlasov model is presented,

paying particular attention to the so-called filamentation problem. In Section 6, the propagation of linear Bernstein modes is treated numerically, in order to show an example of numerical results in a physical context, about a problem of general interest in plasma physics research. In Section 7, the main conclusions of the paper are finally presented.

2. Basic equations

If one considers wavelengths λ much smaller than the electron skin depth, i.e., $4\pi^2c^2/\lambda^2\omega_{pe}^2 = k^2c^2/\omega_{pe}^2 \gg 1$, in which ω_{pe} is the electron plasma frequency, the electrostatic mode is decoupled from the electromagnetic one; under these assumptions, from the Vlasov–Maxwell set of equations one reduces to the Vlasov–Poisson subsystem, which describes the electrostatic part of the spectrum. It is worth noting that, when the wave number is expressed in units of the inverse of the Debye length λ_D, the condition for the validity of the electrostatic approximation is always satisfied for nonrelativistic plasmas, for $k \simeq 1$.

We limit our study at the three-dimensional phase space ($1D - 2V$ phase space). Under these conditions, the basic equations can be written in the following form:

$$\frac{\partial f}{\partial t} + \nabla \cdot (\mathbf{v}f) + \nabla_v \cdot [(\mathbf{E} + \mathbf{v} \times \mathbf{B})f] = \frac{\partial f}{\partial t} + v_x \frac{\partial f}{\partial x} + (E_x + v_y B_0)\frac{\partial f}{\partial v_x} - v_x B_0 \frac{\partial f}{\partial v_y} = 0, \tag{1}$$

$$\frac{\partial E_x}{\partial x} = \int f \, \mathrm{d}v_x \, \mathrm{d}v_y - 1, \tag{2}$$

where $f(x, v_x, v_y, t)$ is the electron distribution function; the ions are considered as a motionless background of neutralizing positive charge, because they cannot take part in the high frequency plasma oscillations. $\mathbf{E}(x, t)$ is the electric field and the magnetic field $\mathbf{B}_0$ is along the z-direction (only variations in the x-direction are allowed in the physical space).

In the previous system, the time is normalized to the inverse of the electron plasma frequency ω_{pe} and the velocity to the electron thermal velocity v_{th}, and consequently, E to $-m\omega_{pe}v_{th}/q$ and B_0 to $-m\omega_{pe}c/q$ (c is the speed of light). Finally, f is normalized to the equilibrium particle density n_0.

In the velocity space, we rewrite the above Vlasov equation in polar coordinates $(v_\perp, \varphi)$, using the expression for the divergence ∇_v in cylindric geometry:

$$\frac{\partial f}{\partial t} + v_x \frac{\partial f}{\partial x} - B_0 \frac{\partial f}{\partial \varphi} + \frac{1}{v_\perp}\frac{\partial}{\partial v_\perp}[v_\perp E_{v_\perp}(\varphi) f] + \frac{1}{v_\perp}\frac{\partial}{\partial \varphi}[E_\varphi(\varphi) f] = 0, \tag{3}$$

$$\frac{\partial E_x}{\partial x} = \rho(x) = \int f v_\perp \, \mathrm{d}v_\perp \, \mathrm{d}\varphi - 1, \tag{4}$$

where $f = f(x, v_\perp, \varphi, t)$, $v_\perp = \sqrt{v_x^2 + v_y^2}$ and $\varphi = \arctan(v_y/v_x)$. The electric field components, in cylindrical geometry, are $E_\varphi(\varphi) = -E_x \sin\varphi$ and $E_v(\varphi) = E_x \cos\varphi$. In the physical space, we impose periodic boundary conditions, so the Poisson equation is integrated using a standard fast Fourier transform routine.

2.1. Splitting method

The numerical integration of the previous system is based on the well-known splitting scheme, which allows to split the evolution of the distribution function in the phase space into two steps, one in the physical space, the other in the velocity. In order to understand the concept underlying the splitting method, one can imagine to move from a generic point a to a generic point b, in the phase space, not going straight on, but taking a *staircase* way. So, from the Vlasov equation (3), we can split the evolution of the distribution function in the following way:

$$\frac{\partial f_x}{\partial t} + v_x \frac{\partial f_x}{\partial x} = 0, \tag{5}$$

$$\frac{\partial f_v}{\partial t} - B_0 \frac{\partial f_v}{\partial \varphi} + \frac{1}{v_\perp} \frac{\partial}{\partial v_\perp} [v_\perp E_{v_\perp}(\varphi) f_v] + \frac{1}{v_\perp} \frac{\partial}{\partial \varphi} [E_\varphi(\varphi) f_v] = 0. \tag{6}$$

The solutions of Eqs. (5) and (6) can be written as follows:

$$f_x(t + \Delta t) = \Lambda_x(\Delta t) f_x(t),$$
$$f_v(t + \Delta t) = \Lambda_v(\Delta t) f_v(t),$$

where Λ_x and Λ_v will be called "translation" operators and whose explicit expression will be evaluated in the next section.

The splitting method provides a solution of Eq. (3), split into (5) and (6), in the following form [6]:

$$f(n\Delta t) = [\Lambda_x(\Delta t/2)\Lambda_v(\Delta t)\Lambda_x(\Delta t/2)]^n f(0) = \Lambda_x(\Delta t/2)\Lambda_v(\Delta t)[\Lambda_x(\Delta t)\Lambda_v(\Delta t)]^{n-1}\Lambda_x(\Delta t/2) f(0) + o(\Delta t^3)$$

correct at second order in time, as discussed in [2].

The formula above allows to highlight the interest of the cylindrical approach with respect to the cartesian one. In fact, the main difference between cylindrical and cartesian scheme, in the integration of the Vlasov equation, arises in the way to implement the splitting method, in velocity space. While in cartesian geometry a subsplitting is needed in the velocity space in order to obtain a symplectic scheme (see [6]), in cylindrical geometry, we do not split the evolution of the distribution function along $v_\perp$ and φ. In polar coordinates, the circular motion is described by a simple translation along the azimuthal angle, with constant velocity ($v_\perp$ = const.). Therefore, the scheme is intrinsically symplectic, because the quantity $v_\perp^2$ (the energy) is perfectly conserved, without any splitting in the velocity space. Then, we obtain naturally a symplectic algorithm and, at the same time, significatively simplify the scheme, from the point of view of the code implementation, with respect to the cartesian case. This could be particularly effective especially in a phase space of higher dimension, from the point of view of the code execution time.

2.2. Hyperbolic equations of conservation law type

Eqs. (5) and (6) can be written in the general form of conservation law:

$$\frac{\partial f}{\partial t} + \nabla \cdot (Af) = 0. \tag{7}$$

The previous equation is known as hyperbolic equation of conservation law type. It is well known that, using a finite difference centered scheme, to evaluate the derivatives in Eq. (7), the algorithm is not stable numerically [7,8], and the remedy for this problem of stability is to use a noncentered approximation for the first order derivatives, the direction of these noncentered differences being determined by the sign of A.

In particular, if the information moves in the positive x-direction (i.e., $A > 0$), we obtain the value of the function f at the point $x_i + \epsilon$ as:

$$f(x_i + \epsilon) \simeq f(x_i) + \epsilon \left(\frac{\partial f}{\partial x}\right)_{x=x_i} \tag{8}$$

otherwise ($A < 0$):

$$f(x_i + \epsilon) \simeq f(x_{i+1}) - (\Delta x - \epsilon) \left(\frac{\partial f}{\partial x}\right)_{x=x_{i+1}}. \tag{9}$$

We can refer to the previous formulas as first order *upwind Taylor expansions*.

It is easily shown that, using an upwind scheme in solving conservation law hyperbolic equations, as the Van Leer's scheme we will describe in the next section [9–13], the algorithm is stable if $\Delta t \leqslant \Delta x/|A|$, which is the well-known Courant–Friedrichs–Lewy condition [7]. In the previous expression, Δt and Δx are the time step and the mesh size, respectively.

3. Integration of the Vlasov equation

3.1. Physical space

The evolution of the distribution function in the physical space is described by Eq. (5). We discretize the plane (x,t) as $x_i = (i-1)\Delta x$ (with $i = 1, N$), $t_n = n\Delta t$, where i and n are integers. The simulation box is given by $[0, L_x]$, and it is divided in N intervals $I_i \equiv [x_i - \Delta x/2, x_i + \Delta x/2]$; so, $\Delta x = L_x/N$.

We define the average value of the function f over a generic interval I_i, at the time t, by:

$$\bar{f}(x_i) = \frac{1}{\Delta x}\int_{x_i-\frac{\Delta x}{2}}^{x_i+\frac{\Delta x}{2}} f(x')\,\mathrm{d}x'. \tag{10}$$

We now integrate Eq. (5) in time over the interval $[t, t+\Delta t]$, after calculating the average value of (5) over I_i, using the definition (10):

$$\bar{f}(x_i, t+\Delta t) = \bar{f}(x_i,t) - \frac{v}{\Delta x}\int_t^{t+\Delta t}\mathrm{d}t' \int_{x_i-\frac{\Delta x}{2}}^{x_i+\frac{\Delta x}{2}} \frac{\partial}{\partial x} f(x',t')\,\mathrm{d}x'. \tag{11}$$

Note that, in order to use a simpler notation, in the previous and in the next formulas, we replace f_x by f and v_x by v. From Eq. (11), integrating by parts over x, one obtains:

$$\bar{f}(x_i, t+\Delta t) = \bar{f}(x_i,t) - \frac{v}{\Delta x}\int_0^{\Delta t}\mathrm{d}\tau\left[f\left(x_i+\frac{\Delta x}{2}, t+\tau\right) - f\left(x_i-\frac{\Delta x}{2}, t+\tau\right)\right], \tag{12}$$

where $t' = t + \tau$. We can use a first order Taylor expansion to evaluate the value of f at the boundary points of the cell I_i, taking into account the propagation direction of the information, according to the sign of v. For example, for $v > 0$, we have:

$$f\left(x_i+\frac{\Delta x}{2}, t+\tau\right) \simeq f(x_i,t) + \frac{\Delta x}{2}\left(\frac{\partial f}{\partial x}\right)_{x=x_i} + \tau\left(\frac{\partial f}{\partial t}\right)_{t=\tau} \tag{13}$$

and

$$f\left(x_i-\frac{\Delta x}{2}, t+\tau\right) \simeq f(x_{i-1},t) + \frac{\Delta x}{2}\left(\frac{\partial f}{\partial x}\right)_{x=x_{i-1}} + \tau\left(\frac{\partial f}{\partial t}\right)_{t=\tau}. \tag{14}$$

From Eq. (5), we obtain the value of the time derivative of the function f:

$$\frac{\partial f}{\partial t} = -v\frac{\partial f}{\partial x}. \tag{15}$$

So, we can replace the time derivative of the distribution function by its spatial derivative. Finally, for $v > 0$, we obtain:

$$f\left(x_i+\frac{\Delta x}{2}, t+\tau\right) \simeq f(x_i,t) + \frac{\Delta x}{2}\left(\frac{\partial f}{\partial x}\right)_{x=x_i} - \tau v\left(\frac{\partial f}{\partial x}\right)_{x=x_i} \tag{16}$$

and

$$f\left(x_i-\frac{\Delta x}{2},t+\tau\right)\simeq f(x_{i-1},t)+\frac{\Delta x}{2}\left(\frac{\partial f}{\partial x}\right)_{x=x_{i-1}}-\tau v\left(\frac{\partial f}{\partial x}\right)_{x=x_{i-1}}. \tag{17}$$

In the same way, one can treat the case $v<0$:

$$f\left(x_i+\frac{\Delta x}{2},t+\tau\right)\simeq f(x_{i+1},t)-\frac{\Delta x}{2}\left(\frac{\partial f}{\partial x}\right)_{x=x_{i+1}}-\tau v\left(\frac{\partial f}{\partial x}\right)_{x=x_{i+1}} \tag{18}$$

and

$$f\left(x_i-\frac{\Delta x}{2},t+\tau\right)\simeq f(x_i,t)-\frac{\Delta x}{2}\left(\frac{\partial f}{\partial x}\right)_{x=x_i}-\tau v\left(\frac{\partial f}{\partial x}\right)_{x=x_i}. \tag{19}$$

We take the first order Taylor expansion for the function f around the grid point x_i and calculate the average value of f:

$$\bar{f}_i=f(x_i)+\mathrm{o}(\Delta x^2). \tag{20}$$

Therefore, if one defines $\sigma_v=\mathrm{sign}(v)$ and $\alpha=(1-\sigma_v)/2$, it is possible to re-write the upwind Taylor expansions as follows:

$$f\left(x_i+\frac{\Delta x}{2},t+\tau\right)\simeq \bar{f}_{i+\alpha}+\sigma_v\frac{\Delta x}{2}\left(\frac{\partial \bar{f}}{\partial x}\right)_{i+\alpha}-\tau v\left(\frac{\partial \bar{f}}{\partial x}\right)_{i+\alpha} \tag{21}$$

and

$$f\left(x_i-\frac{\Delta x}{2},t+\tau\right)\simeq \bar{f}_{i-1+\alpha}+\sigma_v\frac{\Delta x}{2}\left(\frac{\partial \bar{f}}{\partial x}\right)_{i-1+\alpha}-\tau v\left(\frac{\partial \bar{f}}{\partial x}\right)_{i-1+\alpha}. \tag{22}$$

In the previous formulas it is:

$$\left(\frac{\partial \bar{f}}{\partial x}\right)_i=\frac{\bar{f}_{i+1}-\bar{f}_{i-1}}{2\Delta x}. \tag{23}$$

Finally, using the above expansions in Eq. (12), and re-writing in a more compact form the physical space translation operator Λ_x, the evolution of f can be written as follows:

$$\bar{f}_i(t+\Delta t)=\sum_{j=-2}^{1}[\delta_{0,j+\alpha}+A_j(Q)]\bar{f}_{i+j+\alpha}(t), \tag{24}$$

where $Q=v\Delta t/\Delta x$ and:

$$A_{-2}=-\frac{Q}{4}(\sigma_v-Q), \tag{25}$$

$$A_{-1}=Q+\frac{Q}{4}(\sigma_v-Q), \tag{26}$$

$$A_0=-Q+\frac{Q}{4}(\sigma_v-Q), \tag{27}$$

$$A_1=-\frac{Q}{4}(\sigma_v-Q). \tag{28}$$

Eq. (24) is known as *Van Leer's scheme* [9–13] and it is in the form of a conservation law; in fact it is simple to verify that:

$$\sum_{j=-2}^{1}[\delta_{0,j+\alpha}+A_j(Q)]=1. \tag{29}$$

The previous scheme is correct at second order in Δt and Δx [6,13].

3.2. Velocity space

In the velocity space, we discretize the domain, using the cylindrical geometry. In Fig. 1, the numerical velocity grid is shown. Along the azimuthal direction, we divide the domain in N_φ intervals $I_l \equiv [\varphi_l - \Delta\varphi/2, \varphi_l + \Delta\varphi/2]$, where $\varphi_l = (l-1)\Delta\varphi$, $l = 1, N_\varphi$ and $\Delta\varphi = 2\pi/N_\varphi$. Along the radial direction, we consider N_k intervals $I_k \equiv [v_k - \Delta v/2, v_k + \Delta v/2]$, where $v_k = k\Delta v$, $k = 0, N_k$ and $\Delta v = V_{\max}/N_k$. In the previous expressions, we have put $v = v_\perp$, to use a simpler notation and f_v will be replaced by f.

The integration of the Vlasov equation in the velocity space is conceptually similar to the one performed in the physical space. Basically, the fundamental step is to evaluate the average value of the distribution function, over the cells which cover the numerical domain. Observing Fig. 1, it is simple to note that for the generic cell $C_{k,l}$ the cell area is $S_{k,l} = v_k \Delta v \Delta\varphi$, on the contrary for the singular cell $C_{0,l}$ the corresponding area is $S_{0,l} = \pi\Delta v^2/4$; so, the cell $C_{0,l}$ needs a particular treatment.

Therefore, we can write the average value of the distribution function, in the following form:

$$\bar{f}(v_k,\varphi_l) = \frac{4}{\pi\Delta v^2}\int_0^{\frac{\Delta v}{2}} v\,\mathrm{d}v \int_0^{2\pi} \mathrm{d}\varphi f(v,\varphi) \quad \text{for } k=0, \tag{30}$$

$$\bar{f}(v_k,\varphi_l) = \frac{1}{v_k\Delta v\Delta\varphi}\int_{v_k-\frac{\Delta v}{2}}^{v_k+\frac{\Delta v}{2}} v\,\mathrm{d}v \int_{\varphi_l-\frac{\Delta\varphi}{2}}^{\varphi_l+\frac{\Delta\varphi}{2}} \mathrm{d}\varphi f(v,\varphi) \quad \text{for } k=1,N_k. \tag{31}$$

Using the same method as in the previous section, we obtain the value of the distribution function at the time step $t + \Delta t$, from the value at t.

3.2.1. Integration for the point $k = 0$

For the singular point $k = 0$, using Eq. (6), we obtain:

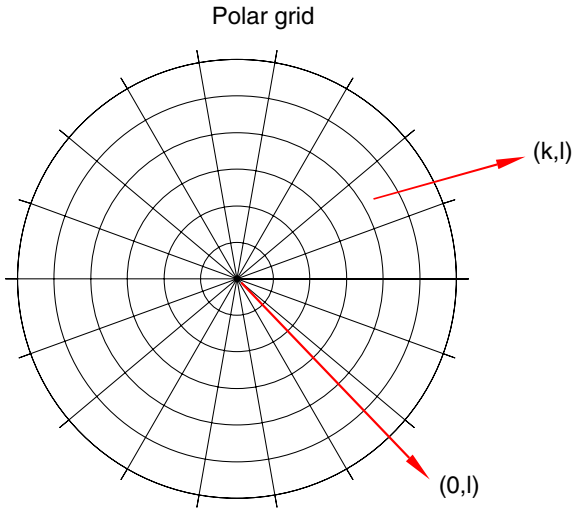

Fig. 1. Cylindrical numerical grid in the velocity space.

$$\bar{f}(v_0,\varphi_l,t+\Delta t)=\bar{f}(v_0,\varphi_l,t)+\frac{4}{\pi\Delta v^2}\int_0^{\Delta t}\mathrm{d}\tau\int_0^{\frac{\Delta v}{2}}v\,\mathrm{d}v\int_0^{2\pi}\mathrm{d}\varphi\left[B_0\frac{\partial f(v,\varphi,t+\tau)}{\partial\varphi}-\frac{1}{v}\frac{\partial}{\partial\varphi}\left(E_\varphi(\varphi)f(v,\varphi,t+\tau)\right)-\frac{1}{v}\frac{\partial}{\partial v}\left(vE_v(\varphi)f(v,\varphi,t+\tau)\right)\right]. \tag{32}$$

In the previous formula, it is easily seen that, because of the periodicity in φ, we have:

$$\int_0^{2\pi}\mathrm{d}\varphi B_0\frac{\partial f}{\partial\varphi}=0 \tag{33}$$

and

$$\int_0^{2\pi}\mathrm{d}\varphi\frac{\partial}{\partial\varphi}\left(E_\varphi(\varphi)f(v,\varphi,t+\tau)\right)=0. \tag{34}$$

Eq. (33) says that the point $k=0$ is not subject to the rotation due to the magnetic field effect; physically, in fact, a particle which is in the point $k=0$ has null velocity and it is not subject to the magnetic force.

Using these considerations and integrating by parts over $\mathrm{d}v$, from Eq. (32), we have:

$$\bar{f}(v_0,\varphi_l,t+\Delta t)=\bar{f}(v_0,\varphi_l,t)-\frac{2}{\pi\Delta v}\int_0^{\Delta t}\mathrm{d}\tau\int_0^{2\pi}\mathrm{d}\varphi E_v(\varphi)f\left(\frac{\Delta v}{2},\varphi,t+\tau\right). \tag{35}$$

Now, we discretize the integral over $\mathrm{d}\varphi$:

$$\bar{f}(v_0,\varphi_l,t+\Delta t)=\bar{f}(v_0,\varphi_l,t)-\frac{2}{\pi\Delta v}\int_0^{\Delta t}\mathrm{d}\tau\sum_{l=1}^{N_\varphi+1}\int_{\varphi_l-\frac{\Delta\varphi}{2}}^{\varphi_l+\frac{\Delta\varphi}{2}}\mathrm{d}\varphi E_v(\varphi)f\left(\frac{\Delta v}{2},\varphi,t+\tau\right) \tag{36}$$

and get

$$\bar{f}(v_0,\varphi_l,t+\Delta t)=\bar{f}(v_0,\varphi_l,t)-\frac{2}{\pi\Delta v}\int_0^{\Delta t}\mathrm{d}\tau\sum_{l=1}^{N_\varphi+1}\int_{-\frac{\Delta\varphi}{2}}^{\frac{\Delta\varphi}{2}}\mathrm{d}\epsilon E_v(\varphi_l+\epsilon)f\left(\frac{\Delta v}{2},\varphi_l+\epsilon,t+\tau\right), \tag{37}$$

where $\varphi=\varphi_l+\epsilon$. Using a first order Taylor expansion, we have:

$$E_v(\varphi_l+\epsilon)\simeq E_v(\varphi_l)+\epsilon\left(\frac{\partial E_v}{\partial\varphi}\right)_{\varphi=\varphi l}=E_v(\varphi_l)+\epsilon E_\varphi(\varphi_l). \tag{38}$$

Taking the Taylor expansion to calculate $f(\Delta v/2,\varphi_l+\epsilon,t+\tau)$, we need the value of the time derivative of f. So, using the same approach as in the previous section, we evaluate the time derivative of the distribution function, by re-writing the Vlasov equation in the velocity space (6) in the following form:

$$\frac{\partial f}{\partial t}=B_0\frac{\partial f}{\partial\varphi}-\mathbf{E}\cdot\frac{\partial f}{\partial\mathbf{v}}. \tag{39}$$

In cylindrical geometry, it is:

$$\frac{\partial}{\partial\mathbf{v}}\equiv\left(\frac{\partial}{\partial v},\frac{1}{v}\frac{\partial}{\partial\varphi}\right) \tag{40}$$

so:

$$\frac{\partial f}{\partial t}=B_0\frac{\partial f}{\partial\varphi}-E_v(\varphi)\frac{\partial f}{\partial v}-\frac{E_\varphi(\varphi)}{v}\frac{\partial f}{\partial\varphi}. \tag{41}$$

We consider now the discretized description and we introduce the following definition:

$$\left(\frac{\partial f}{\partial t}\right)_{k,l} = \left[B_0 - \frac{E_\varphi(\varphi_l)}{v_k}\right]\left(\frac{\partial f}{\partial \varphi}\right)_{k,l} - E_v(\varphi_l)\left(\frac{\partial f}{\partial v}\right)_{k,l}. \tag{42}$$

Therefore, by introducing the quantities $\sigma_l = \mathrm{sign}[E_v(\varphi_l)]$ and $\beta = (1 - \sigma_l)/2$, we can perform the first order upwind Taylor expansions for the distribution function:

$$f\left(\frac{\Delta v}{2}, \varphi_l + \epsilon, t + \tau\right) \simeq f(v_\beta, \varphi_l, t) + \sigma_l \frac{\Delta v}{2}\left(\frac{\partial f}{\partial v}\right)_{v=v_\beta,\varphi=\varphi_l} + \epsilon\left(\frac{\partial f}{\partial \varphi}\right)_{v=v_\beta,\varphi=\varphi_l} + \tau\left(\frac{\partial f}{\partial t}\right)_{v=v_\beta,\varphi=\varphi_l}.$$

From Eq. (37), neglecting the terms containing ϵ^2 and $\epsilon\tau$ (to obtain the second order accuracy in space and time) and taking into account that $\bar{f}_{k,l} \simeq f(v_k, \varphi_l)$ (at first order in the mesh size) and:

$$\int_{-\frac{\Delta\varphi}{2}}^{\frac{\Delta\varphi}{2}} \epsilon \, \mathrm{d}\epsilon = 0, \tag{43}$$

we obtain the expression for $f_v(t + \Delta t)$, as $\Lambda_v^0 f_v(t)$:

$$\bar{f}_{0,l}(t + \Delta t) = \bar{f}_{0,l}(t) - \frac{2\Delta t \Delta\varphi}{\pi \Delta v} \sum_{l=1}^{N_\varphi+1} \left\{ E_v(\varphi_l)\left[\bar{f}_{\beta,l} + \sigma_l \frac{\Delta v}{2}\left(\frac{\partial \bar{f}}{\partial v}\right)_{\beta,l} + \frac{\Delta t}{2}\left(\frac{\partial \bar{f}}{\partial t}\right)_{\beta,l}\right]\right\}. \tag{44}$$

Obviously, in the previous formula, we have:

$$\left(\frac{\partial \bar{f}}{\partial v}\right)_{k,l} = \frac{\bar{f}_{k+1,l} - \bar{f}_{k-1,l}}{2\Delta v}, \tag{45}$$

$$\left(\frac{\partial \bar{f}}{\partial \varphi}\right)_{k,l} = \frac{\bar{f}_{k,l+1} - \bar{f}_{k,l-1}}{2\Delta \varphi}. \tag{46}$$

3.2.2. Integration for the points k = 1, N_k

For the integration of the Vlasov equation, over the grid points $k = 1, N_k$, we use the same approach, which has been described in the previous section, but in this case the shape of the generic grid cell $C_{k,l}$ is different and the definition (31) must be used to calculate the average value of the distribution function.

The value of the function f at the time instant $t + \Delta t$, using Eq. (6), is given by:

$$\bar{f}(v_k, \varphi_l, t + \Delta t) = \bar{f}(v_k, \varphi_l, t) + \frac{1}{v_k \Delta v \Delta \varphi} \int_0^{\Delta t} \mathrm{d}\tau \int_{v_k - \frac{\Delta v}{2}}^{v_k + \frac{\Delta v}{2}} v \, \mathrm{d}v \int_{\varphi_l - \frac{\Delta\varphi}{2}}^{\varphi_l + \frac{\Delta\varphi}{2}} \mathrm{d}\varphi \left[B_0 \frac{\partial f(v, \varphi, t + \tau)}{\partial \varphi} - \frac{1}{v}\frac{\partial}{\partial \varphi}\left(E_\varphi(\varphi) f(v, \varphi, t + \tau)\right) - \frac{1}{v}\frac{\partial}{\partial v}\left(v E_v(\varphi) f(v, \varphi, t + \tau)\right)\right]. \tag{47}$$

In the previous expression, we have the sum of three integrals, $\bar{f}(v_k, \varphi_l, t + \Delta t) = \bar{f}(v_k, \varphi_l, t) + I_1 + I_2 + I_3$; we consider each term of the sum separately. If we put $v = v_k + \eta$ and integrate by parts over φ, the first term gets:

$$I_1 = \frac{B_0}{v_k \Delta v \Delta \varphi} \int_0^{\Delta t} \mathrm{d}\tau \int_{-\frac{\Delta v}{2}}^{\frac{\Delta v}{2}} (v_k + \eta) \, \mathrm{d}\eta \left[f\left(v_k + \eta, \varphi_l + \frac{\Delta\varphi}{2}, t + \tau\right) - f\left(v_k + \eta, \varphi_l - \frac{\Delta\varphi}{2}, t + \tau\right)\right]. \tag{48}$$

If we introduce, as usual, the quantities $\sigma_B = \mathrm{sign}(B_0)$ and $\gamma = (1 - \sigma_B)/2$, we can introduce the upwind Taylor expansions:

$$f\left(v_k+\eta,\varphi_l+\frac{\Delta\varphi}{2},t+\tau\right)\simeq f(v_k,\varphi_{l+\gamma},t)+\eta\left(\frac{\partial f}{\partial v}\right)_{v=v_k,\varphi=\varphi_{l+\gamma}}+\sigma_B\frac{\Delta\varphi}{2}\left(\frac{\partial f}{\partial\varphi}\right)_{v=v_k,\varphi=\varphi_{l+\gamma}}+\tau\left(\frac{\partial f}{\partial t}\right)_{v=v_k,\varphi=\varphi_{l+\gamma}}$$

and

$$f\left(v_k+\eta,\varphi_l-\frac{\Delta\varphi}{2},t+\tau\right)\simeq f(v_k,\varphi_{l-1+\gamma},t)+\eta\left(\frac{\partial f}{\partial v}\right)_{v=v_k,\varphi=\varphi_{l-1+\gamma}}+\sigma_B\frac{\Delta\varphi}{2}\left(\frac{\partial f}{\partial\varphi}\right)_{v=v_k,\varphi=\varphi_{l-1+\gamma}}+\tau\left(\frac{\partial f}{\partial t}\right)_{v=v_k,\varphi=\varphi_{l-1+\gamma}}.$$

Finally, taking into account that:

$$\int_{-\frac{\Delta v}{2}}^{\frac{\Delta v}{2}}\eta\,\mathrm{d}\eta=0 \tag{49}$$

and neglecting the term in η^2 and $\eta\tau$, if one considers that $\bar{f}_{k,l}\simeq f(v_k,\varphi_l)$ (at first order in the mesh size), it is:

$$I_1=\frac{B_0\Delta t}{\Delta\varphi}\left[\bar{f}_{k,l+\gamma}+\sigma_B\frac{\Delta\varphi}{2}\left(\frac{\partial\bar{f}}{\partial\varphi}\right)_{k,l+\gamma}+\frac{\Delta t}{2}\left(\frac{\partial\bar{f}}{\partial t}\right)_{k,l+\gamma}-\bar{f}_{k,l-1+\gamma}-\sigma_B\frac{\Delta\varphi}{2}\left(\frac{\partial\bar{f}}{\partial\varphi}\right)_{k,l-1+\gamma}-\frac{\Delta t}{2}\left(\frac{\partial\bar{f}}{\partial t}\right)_{k,l-1+\gamma}\right]. \tag{50}$$

The numerical integration performed to evaluate the integrals I_2 and I_3 is conceptually the same as for the integral I_1, and the results are in the following form:

$$\begin{aligned}I_2=&-\frac{\Delta t}{v_k\Delta\varphi}\left\{E_\varphi\left(\varphi_l+\frac{\Delta\varphi}{2}\right)\left[\bar{f}_{k,l+\delta_1}+\sigma_1\frac{\Delta\varphi}{2}\left(\frac{\partial\bar{f}}{\partial\varphi}\right)_{k,l+\delta_1}+\frac{\Delta t}{2}\left(\frac{\partial\bar{f}}{\partial t}\right)_{k,l+\delta_1}\right]\right\}\\&+\frac{\Delta t}{v_k\Delta\varphi}\left\{E_\varphi\left(\varphi_l-\frac{\Delta\varphi}{2}\right)\left[\bar{f}_{k,l-1+\delta_2}+\sigma_2\frac{\Delta\varphi}{2}\left(\frac{\partial\bar{f}}{\partial\varphi}\right)_{k,l-1+\delta_2}+\frac{\Delta t}{2}\left(\frac{\partial\bar{f}}{\partial t}\right)_{k,l-1+\delta_2}\right]\right\}\end{aligned} \tag{51}$$

and

$$\begin{aligned}I_3=&-\frac{\Delta t}{v_k\Delta v}\left\{\left(v_k+\frac{\Delta v}{2}\right)E_v(\varphi_l)\left[\bar{f}_{k+\delta_3,l}+\sigma_3\frac{\Delta v}{2}\left(\frac{\partial\bar{f}}{\partial v}\right)_{k+\delta_3,l}+\frac{\Delta t}{2}\left(\frac{\partial\bar{f}}{\partial t}\right)_{k+\delta_3,l}\right]\right\}\\&+\frac{\Delta t}{v_k\Delta v}\left\{\left(v_k-\frac{\Delta v}{2}\right)E_v(\varphi_l)\left[\bar{f}_{k-1+\delta_3,l}+\sigma_3\frac{\Delta v}{2}\left(\frac{\partial\bar{f}}{\partial v}\right)_{k-1+\delta_3,l}+\frac{\Delta t}{2}\left(\frac{\partial\bar{f}}{\partial t}\right)_{k-1+\delta_3,l}\right]\right\}.\end{aligned} \tag{52}$$

In the previous formulas, we have used the definition (42) and the quantities:

$$\begin{aligned}&\sigma_1=\mathrm{sign}\left[E_\varphi\left(\varphi_l+\frac{\Delta\varphi}{2}\right)\right],\quad \delta_1=\frac{1-\sigma_1}{2},\\&\sigma_2=\mathrm{sign}\left[E_\varphi\left(\varphi_l-\frac{\Delta\varphi}{2}\right)\right],\quad \delta_2=\frac{1-\sigma_2}{2},\\&\sigma_3=\mathrm{sign}[E_v(\varphi_l)],\quad \delta_3=\frac{1-\sigma_3}{2}.\end{aligned}$$

Finally, to summarize the numerical advance, the value of the function f_v at the time step $t+\Delta t$, obtained as $\Lambda_v f(t)$, can be written in the following form:

$$\bar{f}_{k,l}(t+\Delta t)=\bar{f}_{k,l}(t)+I_1+I_2+I_3. \tag{53}$$

Note that, in order to calculate the value of the electric field azimuthal component E_φ, at the grid points $\varphi_l \pm \frac{\Delta\varphi}{2}$, we have introduced a new cylindrical numerical grid staggered with respect to the previous one, shown in Fig. 1.

4. Accuracy tests on the cylindrical Vlasov–Poisson code

Using a kinetic code in the study of the wave–particle interaction, the collisionless electric energy dissipation is the most important physical phenomena, in the time dynamics of the system. Therefore, it is fundamental to be able to control the effects of fake numerical dissipation, which plays a role in the transition between continuous and discrete description. In this section, we investigate the properties of the general Vlasov equation and we discuss the time rate change of several quantities, illustrating their conservation in time. These considerations will be useful to test the numerical accuracy of the cylindrical Vlasov–Poisson code and to show that the numerical results are reliable.

4.1. Properties of the Vlasov equation and conservation laws

As it is well known, an ideal Vlasov plasma has got a group of conservation properties, whose mathematical justification can be obtained just by simple considerations on the Vlasov equation. In order to introduce the most important of them, we now show a list of conservation principles, which we will use to verify the numerical accuracy of the kinetic code. Let us consider the general form of the Vlasov equation, which describes the time evolution of the distribution function, for the specie α:

$$\left[\frac{\partial}{\partial t} + \mathbf{v}\cdot\nabla + \frac{q_\alpha}{m_\alpha}\left(\mathbf{E} + \frac{\mathbf{v}\times\mathbf{B}}{c}\right)\cdot\nabla_v\right] f_\alpha(\mathbf{x},\mathbf{v},t) = 0. \tag{54}$$

It is simple to prove that the time rate change of the total number of particle N is equal to zero, i.e.,

$$\frac{\partial}{\partial t}\int f_\alpha \, d\mathbf{x}\, d\mathbf{v} = 0 \tag{55}$$

as a consequence of directly integrating (54) over the entire system. More generally, using the principle of mathematical induction, one can demonstrate that the Vlasov equation conserves the quantities:

$$N_n = \int f_\alpha^n \, d\mathbf{x}\, d\mathbf{v}, \tag{56}$$

where n is an integer. The above set of time invariants provides a very accurate test to control the numerical dissipation and choose the right number of grid points to use, in order to numerically describe the physical phenomena under study.

On the other hand, one can perform a more efficient check, paying attention to the time evolution of the total energy of the system, in which the physical aspects of the system dynamics are contained. From the Vlasov equation (1), the evolution equations for the moments

$$n = \int f \, d\mathbf{v}, \quad n\mathbf{V} = \int \mathbf{v} f \, d\mathbf{v}, \quad n\epsilon = \frac{1}{2}\int (\mathbf{v}-\mathbf{V})^2 f \, d\mathbf{v}$$

can be derived. In particular, using the fact that periodic boundary conditions are imposed in the physical space, the following energy conservation relation in dimensionless units can finally be obtained:

$$E_K + E_{el} = E_{tot} = \text{const.}, \tag{57}$$

where E_K and E_{el} are, respectively, the kinetic (direct and internal), and electric energies:

$$E_K = \int \left(\frac{1}{2} n \mathbf{V}^2 + n\epsilon\right) \mathrm{d}x, \quad E_{el} = \int \frac{E^2}{2}\, \mathrm{d}x.$$

4.2. Numerical results

We discuss now the scaling of the truncation error with the time step and the mesh size, in order to show that the numerical algorithm is second order accurate in time and space. We present a simple test, in which we consider the effect of uniform electric and magnetic fields ($E_0\mathbf{e}_x$ and $B_0\mathbf{e}_z$) on a spatially inhomogeneous plasma. To test the accuracy of the cylindrical code, we compare the numerical results for the distribution function f at a generic time step n, with the analytical solution $f^{(an)}$. The initial condition is a maxwellian function in the velocity space, over which we impose a perturbation in the physical space, with amplitude A and wave-number k:

$$f(x, v, \varphi, 0) = \frac{\mathrm{e}^{-v^2/2}}{\sqrt{2\pi}}[1 + A\cos(kx)]. \tag{58}$$

At each time step, the numerical error, introduced by the discretization of the domain, is given by $\epsilon \simeq [\Delta t^3 + \Delta x^3 + \Delta v^3 + \Delta\varphi^3]$, for a second order scheme. At the nth time step, the total error ξ is of the order of $n\epsilon$, and is defined as

$$\xi = \sqrt{\frac{\sum_{i=1}^{N_x}\sum_{k=1}^{N_v}\sum_{l=1}^{N_\varphi}[f_{i,k,l} - f_{i,k,l}^{(an)}]^2}{(N_x N_v N_\varphi)}} \sim n\epsilon. \tag{59}$$

Then we study the scaling of the angular coefficient m of the above expression with different values of the simulation parameters (it is worth to be note that all the parameters have been chosen of the same order of magnitude and have been scaled by the same factor, in different runs). In Fig. 2, we show the logarithm of m as a function of the logarithm of Δt. The dashed line in the figure is the best fit of the numerical curve, displayed in the figure by dots. The angular coefficient of the dashed line is $\mu \simeq 3.4$, and the same behavior (not shown here) has been obtained for the scaling with Δx, Δv and $\Delta\varphi$. Therefore, from the above results, we can conclude that the cylindrical algorithm, used in the numerical integration of the Vlasov equation, is second order accurate in space and time.

As a first example of application of the cylindrical Vlasov–Poisson code, we discuss the propagation of electrostatic waves in unmagnetized plasmas. In 1946, Landau, in a seminal paper [14], studied the linear

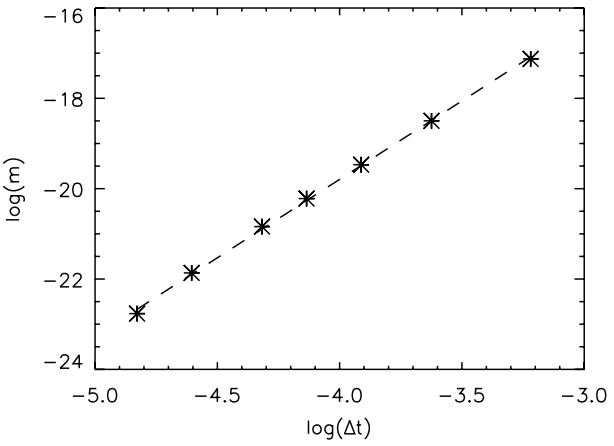

Fig. 2. The scaling of the numerical error with Δt.

solution of the unmagnetized Vlasov–Poisson system of equations; he found that the amplitude of electrostatic perturbations, imposed on a field-free equilibrium, exhibits exponential behavior in time, like $E(t) = E_0 \exp[\gamma_L t]$. The parameter γ_L is proportional to the velocity derivative of the equilibrium distribution function, in the vicinity of the wave phase velocity v_ϕ, i.e. $\gamma_L \propto (\partial f_0/\partial v)_{v=v_\phi}$. In general, for a monotonic decreasing equilibrium distribution function in the velocity space, the wave is exponentially damped in time. The Landau damping rate, obtained for a maxwellian equilibrium distribution, under the assumption of large wavelengths and $v_\phi \gg v_{th}$, is:

$$\gamma_L = -\omega_{pe}\sqrt{\frac{\pi}{8}}\frac{1}{(k\lambda_D)^3}\exp\left[-\frac{1}{2(k\lambda_D)^2}-\frac{3}{2}\right] \tag{60}$$

and $\omega = \omega_{pe}\sqrt{1+3k^2\lambda_D^2}$ is the well-known Bohm–Gross relation [15] for the wave oscillation frequency.

The linear regime of the propagation of electrostatic waves is investigated numerically, considering a case discussed by Filbet et al. [16]. We impose on the system a spatial perturbation of small amplitude ($A = 10^{-2}$) and wave number $k = 0.5$ [the initial condition is given by (58)]. The size of the velocity box is $V_{max} = 4.5$ and outside the velocity simulation interval the distribution function is put equal to zero. The evolution of the initial electric perturbation is followed up to $t_{max} = 40$. We use a number of cells $N_x = 64$, $N_v = 64$ and $N_\varphi = 32$. Then, we compare the numerical solution with the analytical result by Landau. Fig. 3 shows the time evolution of the logarithm of the electric signal; the dashed line represents the theoretical prediction for the amplitude damping. The analytical value for the damping rate is $\gamma_L = 0.1533$, in dimensionless units. It is easy to see from the figure, that the numerical solution is in very good agreement with the analytical one.

At this point, in order to complete the accuracy test on the cylindrical algorithm, we control the conservation of the invariants discussed in the previous sections. We consider the initial condition (58), but increase the number of grid points. Typically, the simulation box is formed by $N_x = 128$ grid points in the physical space and $N_v = 256 \times N_\varphi = 512$, in the velocity. The k-number is $k = 2\pi/L_x$, where L_x is the total length of the x-box; so, we consider only one mode, in the simulation box. Typically, the size of the velocity box is chosen $V_{max} = 6$. In Fig. 4, the time evolution of the invariants N_1 and N_2 is shown for three different values of the external magnetic field. In particular, from the top to the bottom in the figure, we have increasing values of the external field. It is worth to note that the strongly magnetized case displays a better behavior for the time evolution of the invariant N_2, while the conservation of N_1 is well kept independently on the value of B_0.

Also the time evolution of the total energy (see Fig. 5) displays the same behavior discussed before: in the strongly magnetized case, the time evolution of the total energy E_{tot} is more regular than in the case of weak

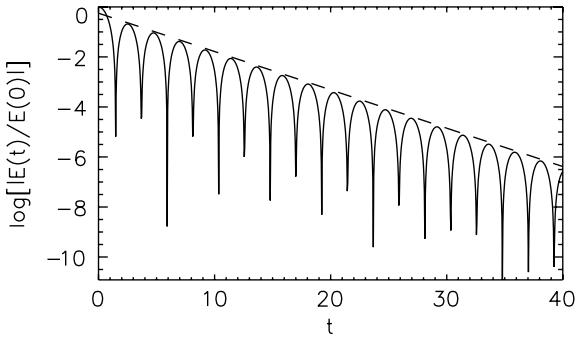

Fig. 3. Time evolution of the logarithm of the electric signal. Comparison between numerical results (solid line) and analytical prediction (dashed line).

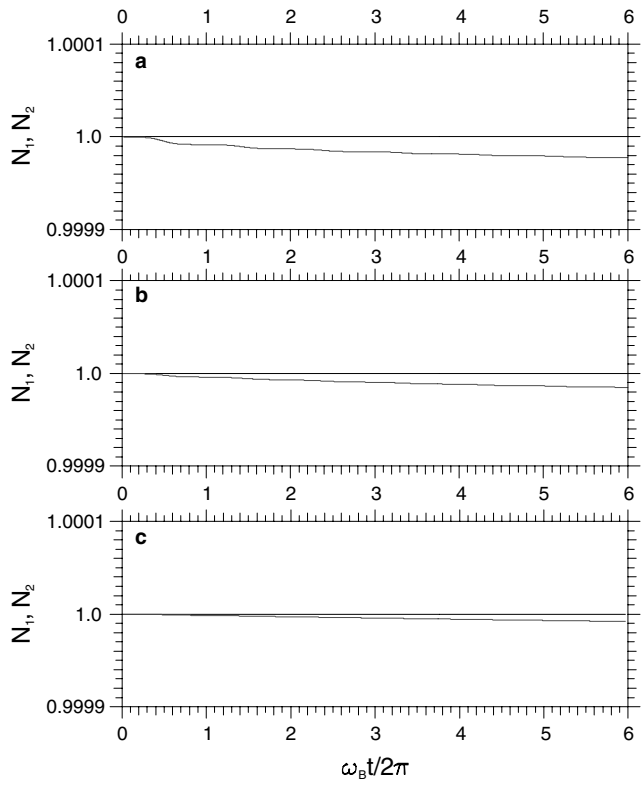

Fig. 4. Time evolution of the invariants $N_1(t)/N_1(0)$ and $N_2(t)/N_2(0)$, as a function of time normalized to the electron cyclotron period ($\omega_B t/2\pi$), for three different values of the external magnetic field $B_0 = 0.0629, 0.085, 0.125$ and for $A = 0.01$.

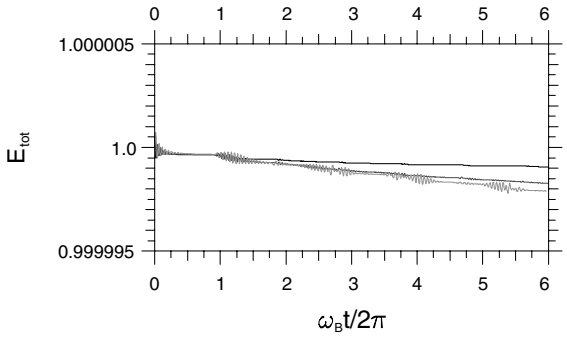

Fig. 5. Time evolution of the total energy $E_{tot}(t)/E_{tot}(0)$, as a function of time normalized to the electron cyclotron period ($\omega_B t/2\pi$), for three different values of the external magnetic field $B_0 = 0.0629, 0.085, 0.125$ and for $A = 0.01$.

magnetic fields. In Fig. 6 we compare the evolution of the electric, kinetic and total energy, for the following set of parameters: $A = 0.03$, $k = 0.405$, and $B_0 = 0.18$. The evolution is followed up to $t = 800\omega_{pe}^{-1}$. In this figure, the fluctuations of the kinetic energy are represented at the top, of the electric energy at the bottom and finally that of the total energy in the middle. While the fluctuations of the kinetic and electric energy are of the order of 10^{-2}, the total energy loss is $|E_{tot}(800) - E_{tot}(0)| = 3 \times 10^{-4}$, about two orders of magnitude

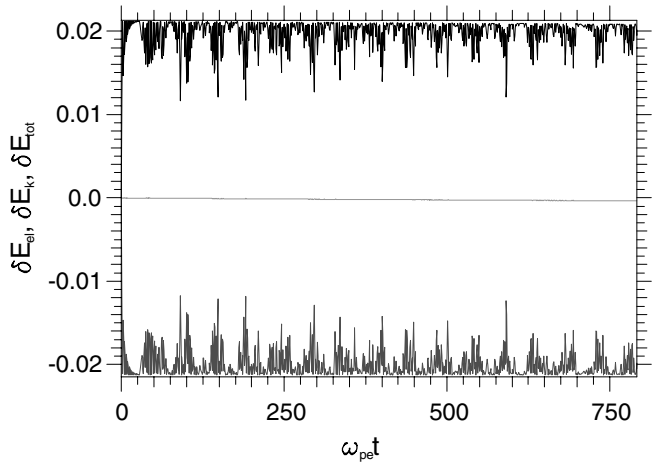

Fig. 6. Long time evolution of the fluctuations of electric energy $\delta E_{el}(t) = E_{el}(t) - E_{el}(0)$, kinetic energy $\delta E_K(t) = E_K(t) - E_K(0)$ and total energy $\delta E_{tot}(t) = E_{tot}(t) - E_{tot}(0)$, for $B_0 = 0.18$, $A = 0.03$ and $k = 0.405$.

smaller than kinetic and electric energy variations. The energy is then conserved all along the simulations and the numerical dissipation is always negligible, with respect to the physical fluctuations.

5. Numerical entropy in Vlasov–Poisson codes and filamentation problem

One of the most important property of a Vlasov plasma concerns the generalization of the Boltzmann H theorem, and in particular the time evolution of the entropy of the system. For a statistical system the entropy is usually defined as:

$$S = -\sum_{\alpha} \int f_{\alpha} \ln f_{\alpha} \, \mathrm{d}\mathbf{x} \, \mathrm{d}\mathbf{v}. \tag{61}$$

By direct and simple substitution, from the Vlasov equation (54), we obtain:

$$\frac{\mathrm{d}S}{\mathrm{d}t} = -\sum_{\alpha} \int \frac{\mathrm{d}f_{\alpha}}{\mathrm{d}t} \ln f_{\alpha} + \frac{\mathrm{d}f_{\alpha}}{\mathrm{d}t} \, \mathrm{d}\mathbf{x} \, \mathrm{d}\mathbf{v} = 0. \tag{62}$$

Thus, entropy is constant in a Vlasov plasma. This is consistent with the fact that the Vlasov treatment neglects the process (binary collision) which causes statistical systems to increase their entropy and evolve toward a Maxwell–Boltzmann distribution. In order to discuss the entropy behavior in a Vlasov model, we first analyze unmagnetized plasmas, where an initial electric modulation (with a small but not vanishing initial amplitude) causes the well-known trapping phenomenon [17] and a nonlinear energy exchange between wave and particles whose velocities are roughly around the wave phase velocity. The particle trapping modifies the shape of the distribution function in the phase space, in the so-called resonant region; as a consequence, the trajectories of the resonant particles become close and small scale structures appear in the phase space.

As well known, kinetic simulations start to induce a bias with respect to the Vlasov equation, when the characteristic length of the phase space structures becomes smaller than the grid resolution [18] (filamentation instability). The inability of such schemes in reproducing the filamentation over small scales causes a topology change in the resonant region of the distribution function because of a dissipative numerical

nonphysical effect, with a consequent entropy increasing, in the nonlinear stage of the system evolution. The situation becomes better increasing the number of the grid points in the numerical domain, but also in the best cases the entropy grows of about 0.1–0.3% at the saturation of the instability, with a simulation box of $N_x = 256 \times N_v = 1024$ points [18].

The magnetized scenario is quite different from the previous. In fact, the introduction of an external magnetic field modifies consistently the features of the wave–particle interaction [19,20], by a detrapping effect on the resonant particles, and prevents the formation of small scale structures in the phase space. Fig. 7 shows the contour plot of the distribution function in the velocity space in two different simulations. The evolution of the system is investigated up $t = 200\omega_{pe}^{-1}$, in the fully nonlinear regime. At the top, we show an unmagnetized run; the perturbation of the f level lines, in the region around the wave phase velocity, is a typical signature of the wave–particle trapping interaction and of the formation of smaller and smaller scale structures. At the bottom, we describe the evolution of the distribution function, under the effect of a strong magnetic field. The distortion of the level lines in the resonant region disappears and the shape of the distribution function is maxwellian. It can easily be seen that the formation of small scale structures is prevented by the introduction of an external field.

Fig. 8 shows the time evolution of the entropy of the system in the unmagnetized run and in the strongly magnetized one. In the first case it is clearly visible that after few time steps the entropy starts growing due to the effect of the trapping phenomenon. On the other hand, the entropy evolution in the second case is

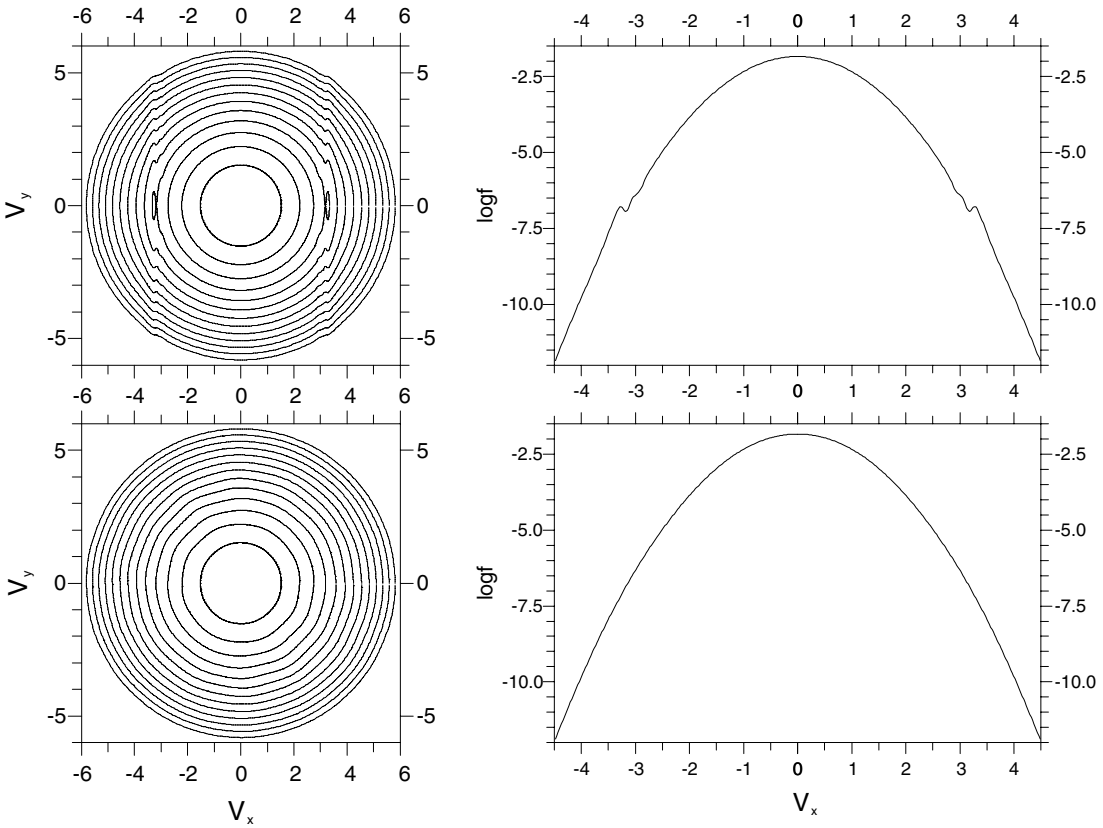

Fig. 7. Velocity space contour plot and semilogarithmic plot of the electron distribution function for $t = 200\omega_{pe}^{-1}$ and for $B = 0$ (at the top), for $B = 0.18$ (at the bottom).

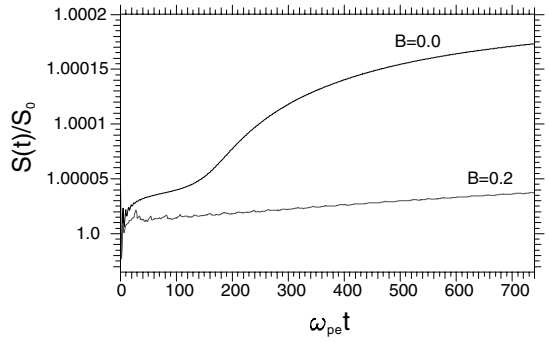

Fig. 8. Time evolution of the entropy $S(t)/S(0)$ is shown for two different values of the magnetic field $B_0 = 0.0$, $B_0 = 0.2$ and for $A = 0.03$.

more regular; we do not observe any increasing in time. The evolution of the entropy exhibits very different behaviors depending on the value of the external field.

Another well known numerical evidence of the filamentation effect is clearly visible in the time evolution of the invariants N_n, for $n > 1$. In particular, when the characteristic size of the phase space structures becomes smaller than the grid resolution, the conservation of the invariants is not kept, but a decreasing appears at the same time instant when the entropy displays the increasing behavior shown in Fig. 8. Since the magnetic field prevents the formation of small structures in the phase space, also the conservation of the invariants is regularly kept, as it is shown in Fig. 9, where a comparison between the unmagnetized case and the strongly magnetized one is presented.

From these considerations, we can conclude that the filamentation problem does not affect kinetic simulations when the magnetic field dominates the dynamics of the system. The wave–particle interaction

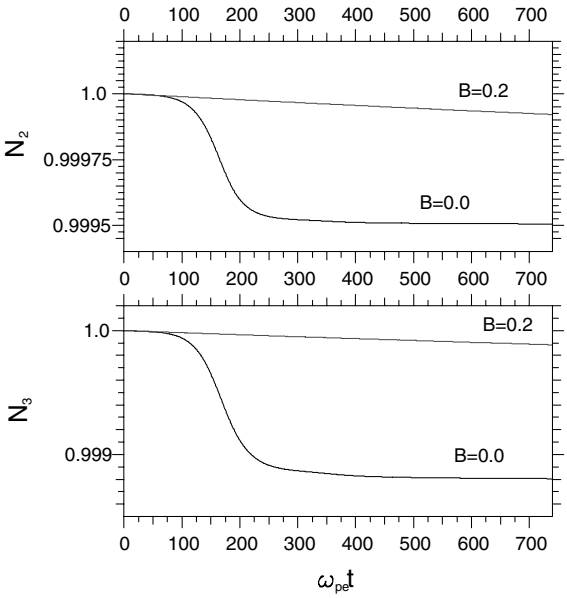

Fig. 9. Time evolution of the invariants $N_2(t)/N_2(0)$ (at the top) and $N_3(t)/N_3(0)$ (at the bottom), as a function of time, for $B_0 = 0.0$ and $B_0 = 0.2$, with $A = 0.03$.

shows different features, but the formation of small scale structures is definitively prevented. This allows to obtain significative numerical results without an extremely refined grid in the velocity space, with respect to the unmagnetized simulations.

6. A test case: the Bernstein–Landau paradox

In this section, we show some numerical results of the cylindrical Vlasov–Poisson code, about the well-known *Bernstein–Landau paradox*, in order to discuss a possible use of the cylindrical algorithm in the physical contest of the propagation of high frequency electrostatic waves. From the linear Landau theory [14] of the electrostatic oscillations in unmagnetized plasma, it is well know that the electric oscillations exhibit exponential damping, caused by the interaction between the wave and particles whose velocity are close to the wave phase velocity. The essence of the Bernstein–Landau paradox is conceptually quite simple: when we consider an external magnetic field, the perpendicular electric oscillations are totally undamped [21], independent of the strength of the background field. It seems that there is a discontinuity between the magnetized and unmagnetized theory.

The Bernstein–Landau paradox was first treated by Baldwin and Rowlands [22], who showed that, when the magnetic field approaches zero, the Bernstein modes behave as usual electrostatic waves in an unmagnetized plasma, because the electron cyclotron frequency decreases with the magnetic field and the cyclotron period becomes smaller than the trapping time of the resonant particles. This causes an overlap of all harmonics of ω_B (the electron cyclotron frequency) and the waves are damped according to the usual Landau damping rate of electrostatic modes, so the Landau's solution is a superposition of many Bernstein modes in the limit $\omega_B \to 0$.

Another analytical and numerical study has been performed by Shukorukov and Stubbe [23], who solved numerically the dispersion relation of the Bernstein waves, and showed that, in the magnetized case, the effect of the Landau damping is visible in the first gyroperiod, for very brief time transients, but the waves are not damped at large times and the amplitude of the oscillations grows with increasing values of the external field. In this way, they solved the problem in linear approximation, paying attention to the time evolution of the density perturbation, under the effects of the magnetic field. The nonlinear propagation has been analyzed numerically by Valentini et al. [19,20].

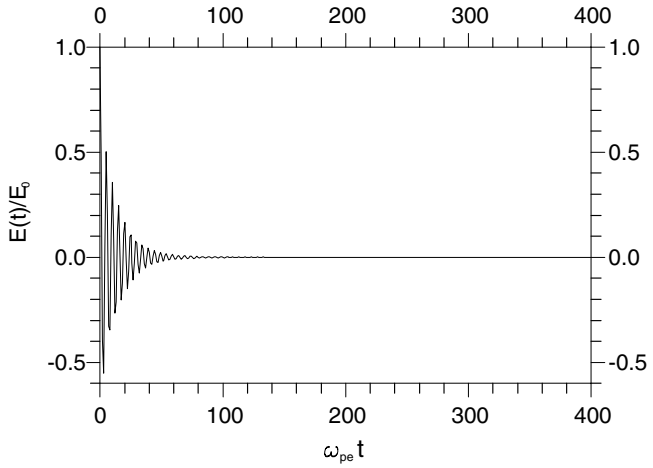

Fig. 10. Time evolution of the electric field $E(t)/E_0$, as a function of normalized time, in the unmagnetized case, $A = 0.01$ and $k \simeq 0.4$.

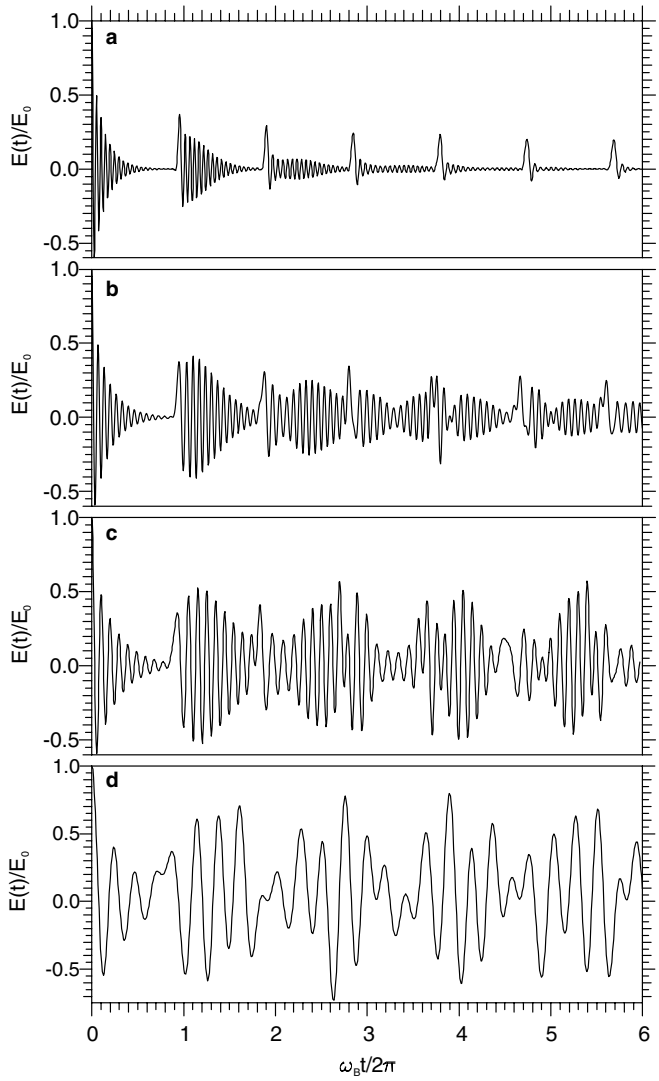

Fig. 11. Time evolution of the electric field $E(t)/E_0$, as a function of time normalized to the electron cyclotron period ($\omega_B t/2\pi$), for $A = 0.01$ and $k \simeq 0.4$, and for four different values of the external field $B = 0.0629, 0.085, 0.125, 0.3$.

We show numerically the linear transition between the magnetized and unmagnetized case, with a brief comparison with the results by Shukorukov and Stubbe. In our simulations, the time evolution of the electrostatic wave is investigated up to 6–10 cyclotron period, in order to investigate in detail the time transient in which the discontinuity appears. As initial condition we consider Eq. (58). In Fig. 10, the time evolution of the electric field is shown in the unmagnetized case, with an initial perturbation amplitude $A = 0.01$ and wave number $k \simeq 0.405$. A typical exponentially damped behavior is clearly visible in the propagation of the wave, and after a time $t \simeq 100$, the electric energy is almost totally dissipated, according to the Landau theory. Fig. 11 shows the effect of an increasing magnetic field on the time oscillations. According to the Shukorukov and Stubbe theory, the effect of the Landau damping is visible in the first gyroperiod, but each cyclotron period the magnetic field raises the electric oscillations and recurrence peaks are strongly visible

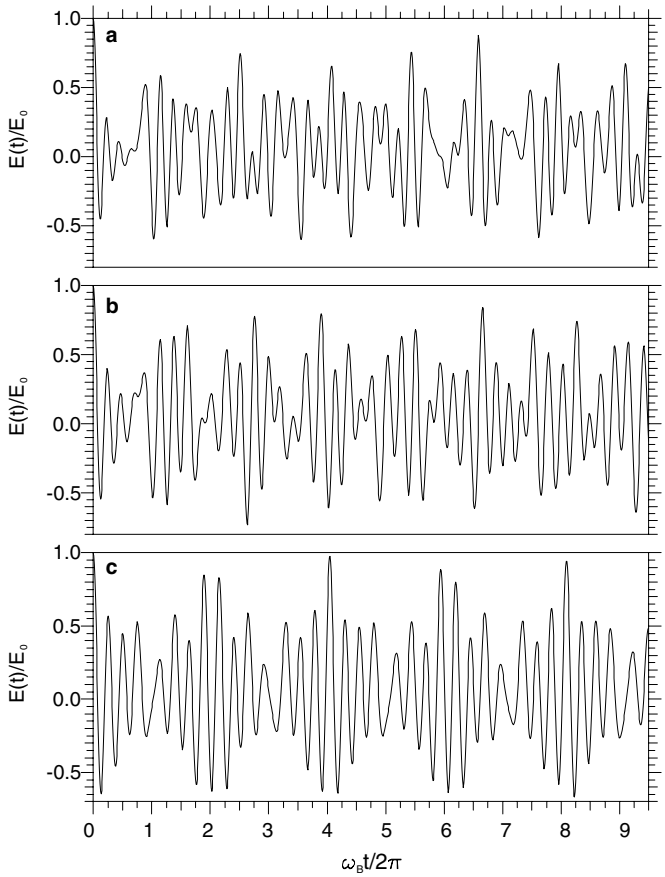

Fig. 12. Time evolution of the electric field $E(t)/E_0$, as a function of time normalized to the electron cyclotron period ($\omega_B t/2\pi$), for $B_0 = 0.3$, $A = 0.01$ and for three different values of the wave number, $k \simeq 0.5$ (a), $k \simeq 0.4$ (b), $k \simeq 0.3$ (c).

in 11(a). As the external field becomes stronger and stronger, the effect of wave damping goes on disappearing, and the amplitude of the oscillations grows, as it simple to see by the comparison between Figs. 11(a) and (c). Finally, in Fig. 11(d), the strongly magnetized case ($B = 0.3$) is shown and undamped electrostatic oscillations are visible. These numerical results are in agreement with the results of Shukorukov and Stubbe in [23].

In correspondence to the strongest value of the magnetic field ($B = 0.3$), in Fig. 12, we have reported the evolution of the electrostatic wave, for three different values of the wave number ($k = 0.5, 0.4, 0.3$). When decreasing the value of k, the oscillations are less and less damped. Actually, as k decreases, according to the Landau's theory [14], the damping rate decreases, since the phase velocity increases and a smaller number of particles interact resonantly with the wave. For $k = 0.3$ [panel (c)], the maximum value of the wave amplitude remains almost equal to the initial wave amplitude.

As it is simple to understand from the results shown in this section, the behavior of the electrostatic oscillations, in magnetized case, is driven by the magnetic field and Landau damping combined effects. The transition between the unmagnetized and the magnetized theories, in the linear as well as in the nonlinear regime, arises in the competition between the cyclotron oscillation and the resonant wave–particle interaction.

7. Conclusions

We have presented a numerical scheme for the solution of the Vlasov–Poisson system of equations in magnetized plasmas. The algorithm is based on the coupling of the splitting method in the phase space in electrostatic approximation and a finite difference upwind scheme, providing the second order accuracy in space and time. The numerical scheme for the integration of the so-called hyperbolic equations has been generalized in cylindrical coordinates, in order to simplify the integration of the velocity space Vlasov equation.

The cylindrical geometry is particularly useful in describing the rotation of the charged particles in the plane perpendicular to the direction of the external uniform magnetic field. The algorithm, we have used in solving numerically the rotation in the velocity space, is a generalization of the well-known Van Leer's scheme and gives us a simpler way (with respect to a cartesian scheme) to advance the electron distribution function on the discretized velocity domain. By comparing the cylindrical algorithm with the cartesian schemes, we have highlighted the main differences between the two different approaches. In particular, no splitting in the velocity space is needed in polar coordinates, with respect to the cartesian case, in order to obtain a symplectic scheme, this resulting in a significative simplification of the algorithm, from the point of view of the code implementation.

Several numerical tests have been described in order to demonstrate that the numerical dissipation does not affect the numerical results (energy conservation tests) and a more detailed study of the time evolution of the entropy in a Vlasov model has been performed. Due to the fact that the magnetic effect prevents the formation of small scale structures in the phase space (peculiar feature of the unmagnetized wave–particle interaction), the magnetized Vlasov codes are not affected by the filamentation phenomenon, when the dynamics of the system is dominated by the magnetic field.

We have shown the numerical results of the cylindrical Vlasov–Poisson code in the study of the time evolution of high frequency electrostatic waves in a uniform magnetic field and, in particular, we have discussed the well-known Bernstein–Landau paradox in linear regime, in order to provide an example of application of the algorithm. Using our kinetic code, it is obviously possible to investigate the nonlinear stage of the wave–particle interaction in a magnetized plasma [19,24] and this work represents a significative step beyond in the study of the kinetic effects on the high frequency plasma oscillations in the presence of an external magnetic field and in particular in the investigation of the transition between the trapped motion of the electrons in the electrostatic potential well (unmagnetized nonlinear wave–particle interaction) and a more complicated particle dynamics, dominated by the coupling of two nonlinear oscillatory motions (trapping motion and cyclotron rotation).

References

[1] C.k. Birdsall, A.B. Langdon, Plasma Physics via Computer simulation, McGraw-Hill, Singapore, 1985.
[2] C.Z. Cheng, G. Knorr, J. Comput. Phys. 22 (1976) 330–351.
[3] E. Fijalkow, Comput. Phys. Commun. 116 (1999) 319–328.
[4] E. Fijalkow, Comput. Phys. Commun. 116 (1999) 329–335.
[5] E. Fijalkow, Comput. Phys. Commun. 116 (1999) 336–344.
[6] A. Mangeney, F. Califano, C. Cavazzoni, P. Travnicek, J. Comput. Phys. 179 (2002) 495.
[7] R. Peyret, T.D. Taylor, Computational Methods for Fluid Flow, Springer, New York, 1983.
[8] E. Godlewski, P.A. Raviart, Numerical Approximation of Hyperbolic System of Conservation Laws, Springer, New York, 1995.
[9] A. Harten, J. Comput. Phys. 135 (1982) 260–278.
[10] A. Harten, J. Comput. Phys. 131 (1986) 3–46.
[11] A. Harten, J. Comput. Phys. 131 (1982) 247–250.
[12] R.J. Leveque, SIAM J. Numer. Anal. 33 (1996) 627–665.
[13] B. Van Leer, J. Comput. Phys. 23 (1976) 263–275.

[14] L.D. Landau, J. Phys. (Moscow) 10 (1946) 25.
[15] N.A. Krall, A.W. Trivelpiece, Principles of Plasma Physics, McGraw-Hill, Kogakusha, 1973.
[16] F. Filbet, E. Sonnendruker, P. Bertrand, J. Comput. Phys. 172 (2001) 166–187.
[17] T. O'Neil, Phys. Fluids 8 (1965) 2255.
[18] M-C. Firpo, F. Doveil, Y. Elskens, P. Bertrand, M. Poleni, D. Guyomarc'h, Phys. Rev. E 64 (2001) 026407-1.
[19] F. Valentini, P. Veltri, A. Mangeney, Phys. Rev. E 71 (2005) 016402.
[20] F. Valentini, P. Veltri, A. Mangeney, Nonlinear evolution of high frequency electrostatic waves in a magnetized plasma: Berstein–Landau paradox revisited, in: G. Bertin, D. Farina, R. Pozzoli, (Eds.), Proceedings of the International Symposium Plasma in the Laboratory and in the Universe: New Insights and New Challenges, Como, Italy, September 2003. AIP Conference Proceedings, vol. 703, p. 80.
[21] I.B. Bernstein, Phys. Rev. 109 (1957) 10.
[22] D.E. Baldwin, G. Rowlands, Phys. Fluids 9 (1966) 2444.
[23] A.I. Sukhorukov, P. Stubbe, Phys. Plasmas 4 (1997) 2497.
[24] C. Marchetto, F. Califano, M. Lontano, Phys. Rev. E 67 (2003) 026450.